Physica B 665 (2023) 415063

Contents lists available at ScienceDirect

Physica B: Condensed Matter

journal homepage: www.elsevier.com/locate/physb

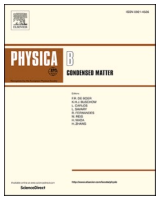

The effect of ZnO:Si_3N_4 nanocomposite interlayer on electrical properties and interface-states between metal-semiconductor in Al/p-Si (MS) structures

Erhan İbrahimoğlu *, Mine Kırkbınar, Fatih Çalışkan, Zafer Tatlı

Department of Metallurgical and Materials Engineering, Faculty of Technology, Sakarya University of Applied Sciences, 54187, Sakarya, Turkey

ARTICLE INFO

Keywords:
MIS structures
Interface-states
Band-gap energy
Diodes

ABSTRACT

In the study, the fabrication processes of the Al/p-Si (MS), Al/ZnO/p-Si (MIS1), and Al/(ZnO:Si_3N_4)/p-Si (MIS2) structures were described and the effect of the ZnO:Si_3N_4 interface layer in MS was investigated in detail. The ZnO and (ZnO:Si_3N_4) thin films were coated on p-Si substrates and annealed at 500 °C for 1 h. Si_3N_4 and ZnO phases were identified via X-ray diffraction (XRD) and Raman spectra. FESEM images demonstrated that ZnO nanorods grew on Si_3N_4 particles with a heterogeneous nucleation mechanism. The I–V characterization was performed in the dark (±4 V). The basic diode parameters (barrier height (BH), series/shunt (R_s/R_{sh}) resistances, rectifying rate (RR=I_f/I_r), and ideality factor (n)) were calculated from various methods. The RR, and R_{sh} values increased, but n, R_s and BH decreased by insulating layer in the MIS2 The energy-dependent profiles of interface-states (N_{ss}) were also extracted from the I–V plots according to voltage-dependent n and BH. The MIS2 provided the best passivation effect with decreasing interface traps.

1. Introduction

In recent years, the demand for the materials included in the wide band gap technologies has increased due to the developments in opto-electronic devices [1]. Among the materials with wide band gap structure, ZnO is preferred in semiconductor devices because it is sensitive to blue light and UV light spectrum [2]. It is used in photonic applications since the band gap of ZnO is 3.37 eV [3]. It has a binding energy of ZnO (60 meV) and allows emission at room temperature (RT) and above [4]. In addition, ZnO has advantages such as high chemical and thermal stability, radiation resistance, and growth at low temperatures [5,6]. ZnO is more active against reduction reactions (it is highly active towards photo-induced redox reaction), biocompatible, environmentally friendly, and shows higher UV emission. Therefore, the ZnO is frequently used in different fields such as light emitting diodes (LEDs) [7] chemical and gas sensors [8], optical waveguides [9], solar cells [10], Schottky diodes [11], laser diodes [12], UV-photodiodes [13]. ZnO structures are easily grown as single crystals and have widely different fabrication methods such as laser deposition, chemical vapor deposition, spray pyrolysis, spin coating, and dip coating. The spin coating method is preferred more than other methods because it provides low-cost, applicable, and homogeneous coating. The performance of ZnO-based instruments depended on impurity atoms, point defects, and Zn transition (electron transition in the band gap) [14,15]. Electron and hole recombination occurs very rapidly on the ZnO surface, resulting in low photogeneration [16]. Moreover, the photo-generated electrons and holes recombine easily on the surface of ZnO, resulting in the poor utilization of photo-generated carriers. In order to prevent electron-hole recombination, the band gap is changed by making metal [17] or non-metal [18,19] additives to the structure, and narrower band gap particles are sensitized [20] by the growth of different morphologies as nanotube [21] and nanodisc [22].

Si_3N_4 has three crystal structures α-Si_3N_4, β-Si_3N_4 and γ-Si_3N_4. α and β-Si_3N_4 are hexagonal and γ-Si_3N_4 is a cubic spinel crystal structure. α-Si_3N_4 was used in optical applications as doping material due to its similar crystal structure with ZnO [23]. The Si–N–Si bonds are given hardness by the necessity of nitrogen forming three bonds rather than two bonds. Nitrogen atoms are roughly arranged in a tetrahedral fashion around silicon. The structures formed by insulating layer coating on semiconductor in optoelectronic devices are called MIS (metal-insulator-semiconductor) [24]. The most fundamental requirements for choosing an insulating material as an interface layer or additive are that it should have a high dielectric constant, be able to passivate the surface, have a controlled current-conducting mechanism, and have a

* Corresponding author.
E-mail address: erhanibrahimoglu@subu.edu.tr (E. İbrahimoğlu).

https://doi.org/10.1016/j.physb.2023.415063
Received 6 March 2023; Received in revised form 28 May 2023; Accepted 10 June 2023
Available online 12 June 2023

low leakage current [25,26]. Recently, nitride-based thin films as an insulating layer collect electrons on it and prevent reverse current flow [27]. The photocatalytic properties of diodes are improved with surface passivation by adding insulating material to the structures. Nitride interlayers prevent the contact of silicon with oxygen and prevent the formation of an oxide layer. In addition, since silicon nitride (5.3 eV) has a narrower band gap than silicon oxide, it shows effective photoluminescence in infrared and visible light [28].

Silicon nitride has been used as an insulating layer to create a good passivation layer between the metal and the contact. On the other hand, Si_3N_4 which has a wide band gap, is transparent in the UV region and a good passivation inhibitor in the IR region. Thanks to its feature in the infrared region, it is one of the materials preferred in applications requiring low optical loss [29,30]. At the same time, the ZnO matrix is suitable for use as a composite, as it will increase the UV resistance of the nitrided structure. The main advantage of Si_3N_4 is its high dielectric permeability and low surface density. Si_3N_4 is used instead of additive in different layers, prevents agglomeration of metal-oxide, behaves in hetero-nucleation centers, and improves electro-optical properties [31]. Si_3N_4 is among the favorite materials of recent times because it has features such as high oxidation resistance, high strength, and thermal stability [32].

In this study, by the addition of Si_3N_4, it is expected that will increase the rectification ratio by reducing the reverse bias current (leakage) with the help of reducing the recombination and activating the movements of the charge carriers [33].

For this aim, the addition of Si_3N_4 into the ZnO matrix was carried out by the sol-gel method. The prepared solution was coated on the surface of the Si substrates at 2000 rpm for 40 s by the spin coating method. Aluminum (Al) ohmic and rectifier contacts were coated in a physical vapor (PVD) device. The Al/ZnO:Si_3N_4/p-Si (MIS2) structure's current-voltage (I–V) characteristics were compared to those of the reference Al/p-Si (MS) and Al/ZnO/p-Si (MIS1) structures that were previously achieved in the dark at room temperature.

2. Materials and methods

Firstly, Al was coated on a p-Si wafer (100 orientation, 1–10 Ωcm resistivity, and 380 μm thickness) by PVD technique to fabricate the reference MS sample that provides metal-semiconductor (MS) heterojunction. After, ZnO NPs were synthesized from zinc acetate dihydrate (ZnAc) precursor powders via sol-gel method and it was stirred in isopropanol at 50 °C for 1 h in a magnetic stirrer. The commercial Si_3N_4 powders in a different beaker were dispersed in isopropanol at RT for 2 h in an ultrasonic bath. Both prepared solutions were mixed for 1 h with the help of ultrasonication at RT. The amount of Si_3N_4 was adjusted so that the stoichiometries as considering ZnO/Si_3N_4 molar ratio 10/0.5. Silicon substrates were cleaned in ethanol, sulfuric acid, and HF, respectively and dried in a nitrogen environment. Then, the final solution was dynamically coated at 2000 rpm for 40 s in the spin coating device on the surface of the cleaned substrates. This process was repeated 10 times and the wafers were annealed at 150 °C for 5 min between each iteration. After the coating process, the coated substrates were annealed at 500 °C for 1 h in order to ensure thin film growth on the surface.

The prepared ZnO and ZnO:Si_3N_4 thin films were coated by an Al rectifier and ohmic contacts for comparison of MS as 150 nm. Fig. 1 shows the schematic image of the fabrication routes of the MIS2 sample.

3. Results and discussion

The fabricated samples were characterized chemically and morphologically by XRD, Raman and FESEM-EDS analysis. Then, the I–V characteristics of them were examined in a dark environment. The XRD diffraction pattern of the MIS2 sample was given in Fig. 2a. As seen in the results, it was observed that the ZnO phase was dominant in the peaks. The 2θ characteristic peaks of the ZnO phase founded at 31.74°, 34.40°, 36.24°, 47.58°, 56.24° and they belong to (100), (002), (101), (102), (110) lattice planes, respectively. These values also corresponded to the JCPDS 36–1451 standard card and hexagonal wurtzite crystal structure of ZnO. In addition, the peaks located at approximately 20.88°, 31.30° and 35.64° were characteristic peaks of α-Si_3N_4 and complied with JCPDS 41–360 standard card. SiO_2 as an impurity phase was not observed in the structure. The XRD results supported the successful fabrication of Si_3N_4:ZnO thin films.

On the other hand, in Fig. 2b, the Raman spectra of ZnO:Si_3N_4 nanocomposite confirmed the presence of required groups and their characteristic stretching-bending vibrations as presented. The peak at 305 cm^{-1} belongs to the ZnO E1 (LO) mode and is due to structural defects and oxygen deficiency [34]. The peak at 438 cm^{-1} that slightly observed belongs to ZnO, which has a hexagonal wurtzite crystal structure. In addition, Si–N bonds formed peaks at 938–1375 cm^{-1} as a result of the contribution of doped Si_3N_4 [35–37]. The peak seen at 522 cm^{-1} could have originated from the silicon substrate since homogeneity is difficult to achieve using the spin coating method due to the centrifugal force. If optimum conditions are obtained with different parameters such as coating thickness, processing time and temperature, the intensity of the peak originating from the substrate can be

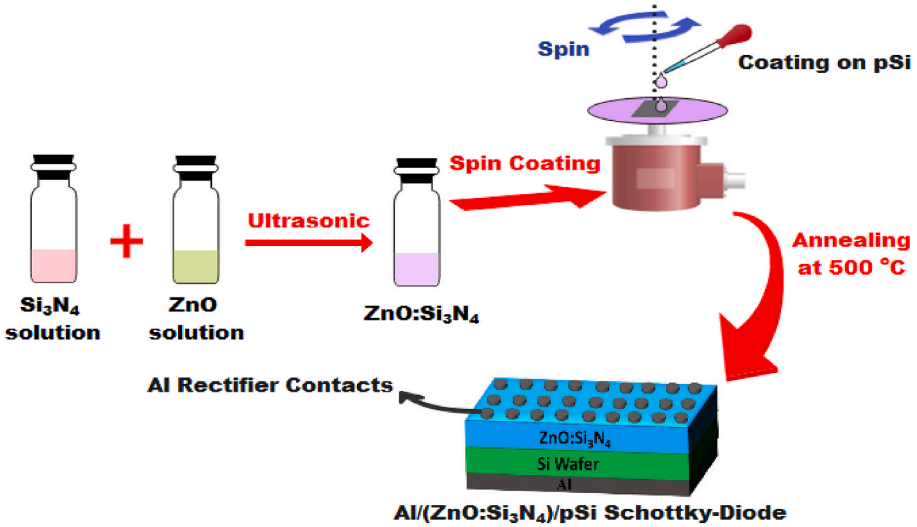

Fig. 1. Fabrication routes of the MIS2 sample.

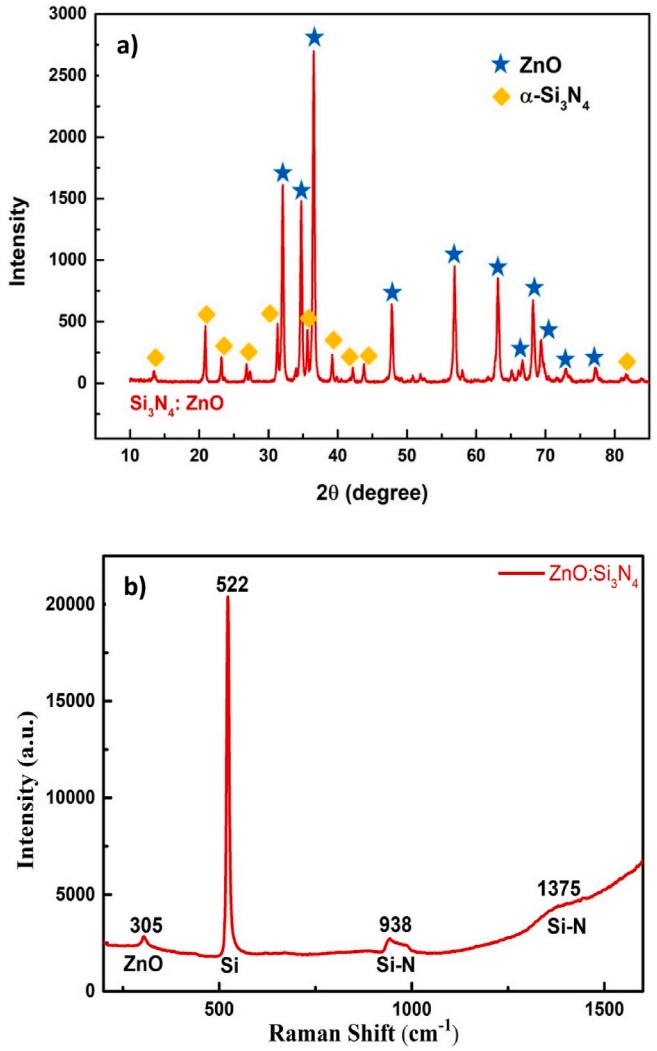

Fig. 2. a) the XRD results and b) Raman spectra of the MIS2.

minimized.

As seen in Fig. 3, the FESEM results of the samples are presented. The grains shown with number 1st define silicon nitride because of the similarity of phase formation and the increase in nitride ratio with the EDS results. Nanorod and sphere-like structures that developed on silicon nitride grains belong to ZnO nanorods. Si_3N_4 grains showed a nucleating effect for the development and allowed the growth of ZnO nanorods. Sharma et al. reported that the ZnO particles exhibited agglomeration-like growth on the Si_3N_4 structure in the form of a triangle-like shape with sharp corners [31]. In the EDS results, it is observed that the presence of N atoms and the decrease in weight percentage of Zn in region 1. It was noted that there was no N atom in the second region and the Zn ratio increased. Examining the tables provided in the EDS spectrum has shown that the first region was Si_3N_4 and the second region was ZnO.

The EDS mapping results are shared in Fig. 4. It is observed that N, O, and Zn atoms are homogeneously distributed in the structure. The surface coating was shown to have a uniform distribution at all points of the silicon substrate.

In order to determine the basic electrical parameters of the prepared SDs, the forward and reverse bias I–V measurements were carried out in the dark with a wide range of bias voltage (±4 V) by 25 mV steps at RT. According to TE theory, the relation between V and I in n the forward bias region can be extracted as follow Eq. (1) [38–41]:

$$I = A.A^{*}.T^{2}\exp\left(-\frac{q\Phi_b}{k.T}\right)\left[\exp\left(\frac{q.Vd}{n.k.T}\right)-1\right] \quad (1)$$

Here, "$A.A^{*}.T^{2}\exp\left(-\frac{q\Phi_b}{k.T}\right)$" terms is the reverse-saturation current (I_o) and is a very important parameter to determine the nature of BH, V_d ($V-IR_s$) is the voltage devolve on the diode, R_s is the series-resistance, k is the Boltzmann constant, T is the absolute temperature in K, n is the ideality factor, Φ_b is the barrier-height, A is the rectifier contact area, and A* is the Richarson constant (for p-Si, $A^{*} = 32\ A\ cm^{-2}\ K^{-2}$) [39–41]. Eq. (1) can be modified as follows by taking the logarithm of both sides and n values can be calculated from the slope of the LnI vs V plots according Eq. (2).

$$LnI(V) = Ln\ I_0 + \left(\frac{q}{nkT}\right)V \quad (2)$$

Fig. 5 (a) and (b) show the semi-logarithmic I vs V plots and R_s vs V plots of the SDs, respectively. Ln(I) vs V plots inset in Fig. 5 (a) and has

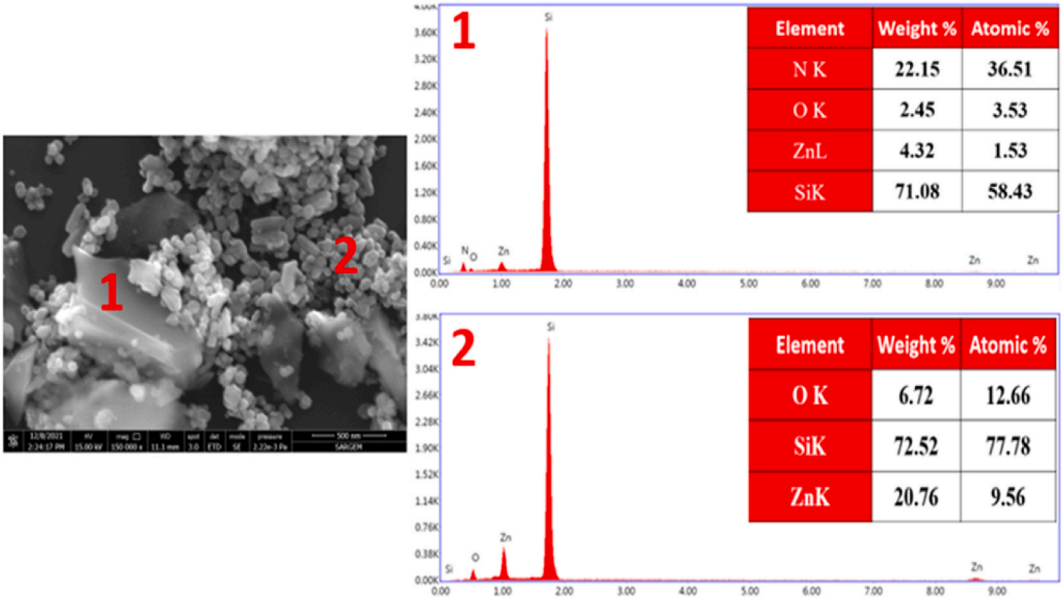

Fig. 3. FESEM images of the MIS2 sample.

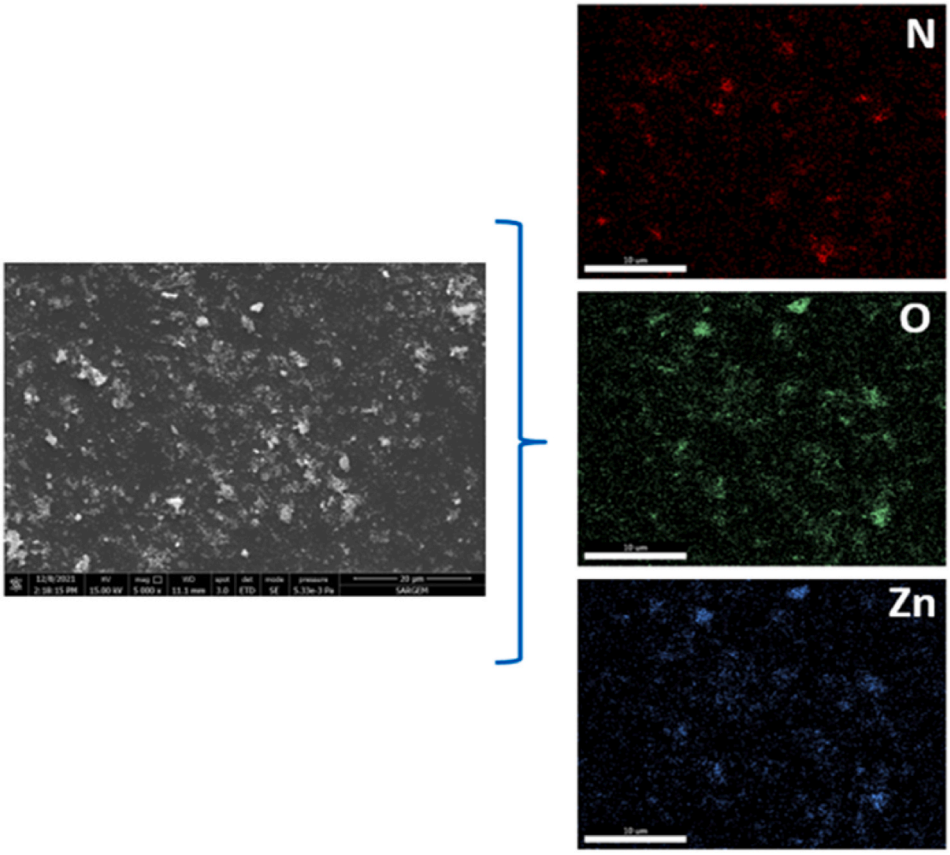

Fig. 4. EDS mapping of the MIS2 sample.

good linear behaviour in the dark. In terms of rectification performance, it has been reported that SDs with thin interface have a rectifier behaviour and the rectification-ratio (RR=I_F/I_R) increases with doping of the Si_3N_4 due to the passivation effect and decreased interface traps [41]. The interior electric field formation to the electron and hole diffusion and applied external electric field have the same direction in the reverse bias region, they have opposite directions in the forward bias region. Mansour et al. [42] reported that a space-charge effect and localized electric field are likely to be strengthened in the p-Si/ZnO junction; so that the dependence of the reverse current on the enhanced electric field will result in an increase in the reserve saturation current of the investigated Ag/ZnO nanofibers/p-Si diodes.

The decrease in I_o with the addition of Si_3N_4 is the result of reducing interface traps under the passivation of oxygen defects into ZnO leads to which is due to Si_3N_4 already formed in as-deposited films. During the re-construction procedure of thin film morphology, the Si_3N_4 nanoparticles and the dopping-induced defects can behave as nucleation centers and excessive Zn^{+2} ions can transport more freely, which leads to the participation of the interface layer [31]. At the same time, the other result extracted from Fig. 5 (a) is that the MIS2 type SD shows a typical rectification behaviour with low turn-on voltage and leakage current. The observed non-saturation in the reverse current can be also rooted in the generation-recombination current, tunneling effect, surface states, and interfacial layer.

Both values of the I_o and n can be calculated from the intercept and slope of the linear part ln(I) vs V (inset in Fig. 5a) plos and then, the value of Φ_b can also be calculated by using these experimental values of I_o and Schottky-contact area (A) as given follows [43,44]:

$$n = \frac{dV}{dlnI}\frac{q}{k.T} \tag{3a}$$

$$\Phi_b = \left(\frac{kT}{q}\right) Ln\left(\frac{A.A^*.T^2}{I_0}\right) \tag{3b}$$

On the other hand, as can be clearly seen in Fig. 5b, the R_{sh} values were decreased in the MIS2 type SD and the diode current is limited due to the increase in R_s with the increase in voltage and ZnO:Si_3N_4 interfacial layer. Because the applied voltage on the diode will be shared between them ($V_a = V_d + V_{Rs} + Vi$). The R_s and R_{sh} values of two-type SDs are extracted from Ohm's Law ($R_i = V_i/I_i$) at enough high forward and reverse bias voltages (±4 V), respectively. The values of basic electric parameters such as R_s, R_{sh}, I_o, n, and Φ_b were found in the dark for all samples that calculated different methods as given in Table 1. It is clear that the MIS2 SD has a low reverse-saturation current, low ideality factor (n), and low BH and hence this is evidence of the best of SD when compared to others.

In this study, the ideality factors of the SDs fabricated from ZnO thin films are similar to the results of metal/ZnO/p-Si MIS type diodes/SDs fabricated by sol-gel spin coating in the literature [45–47]. On the other hand, the presence of a thin film between metal and semiconductor, its thickness, and the inhomogeneities of BH bring about a higher value of the ideality factor. The currents arising from the recombination of carriers in the depletion region or the tunneling effect are also the other reasons for higher n values [48–51].

Another approach to defining both the value of BH and R_s is the Norde method. According to Norde, when the I–V plot has not a distinct linear behaviour for intermediate bias voltage, the obtained value of them from TE theory becomes questionable. For this reason, the modified Norde function (Eq. (4)) for non-ideal cases is determined as follows [39,41];

$$F(V;\alpha) = \frac{V}{\alpha} - \frac{kT}{q} Ln\left(\frac{I(V)}{AA^*T^2}\right) \tag{4}$$

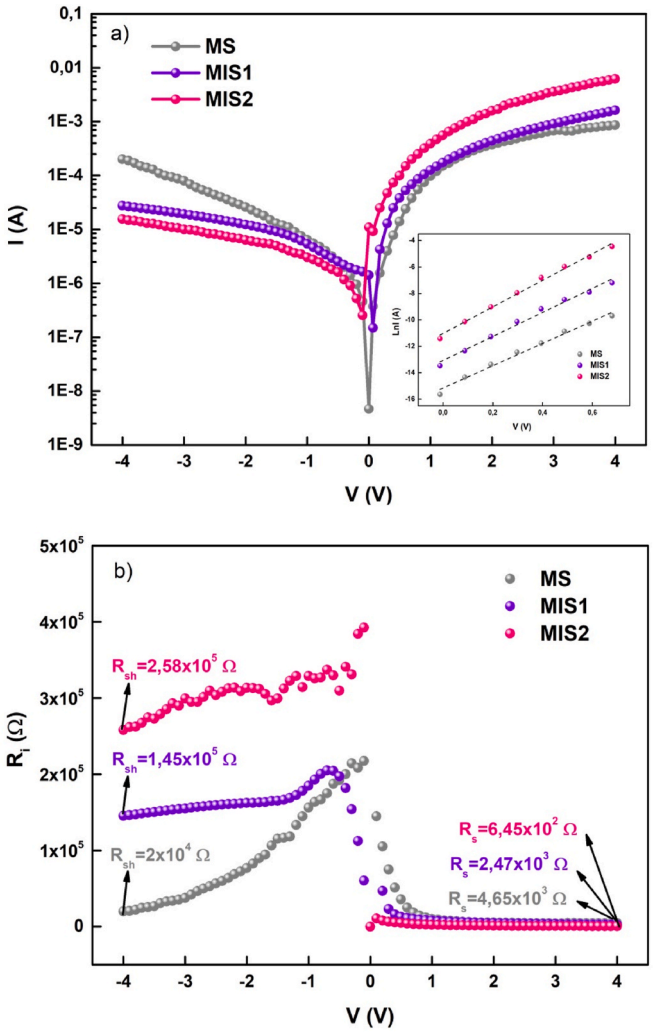

Fig. 5. a) the semi-logarithmic I–V, b) Ri-V curves of the samples in the dark.

Here ***α*** is an integer and must be greater than the "n". F(V;α) vs V plot gives a minimum point when the I–V plot starts to deviate from linearity due to the effects of R_s and interfacial layer. In this case both the value of BH and R_s can be calculated by using minimum values of F_{min} and corresponding voltage and current to the minimum point as given follow Eq. (5) and Eq. (6):

$$\Phi_b = F_{min}(V;\alpha) + \left(\frac{\alpha - n}{n}\right)\left(\frac{V_{min}}{\alpha} - \frac{kT}{q}\right) \tag{5}$$

$$R_s = \frac{kT(\alpha - n)}{qI_{min}} \tag{6}$$

As can be clearly seen in Fig. 6d, the minimum point of the F(V)–V curve has a distinct minimum point for two types SD's in the dark. The value of Φ_b and R_s were calculated using Eqs. (5) and (6), respectively, and also tabulated in Table 2.

The density of N_{ss} offers important data on the conduction mechanism and leads to the higher value of n and tunneling by interface traps. Because, they act as recombination centers and so may capture and release any electron under electric field, illumination, and temperature effects [52].

The values of N_{ss} can be calculated from rearranged Eq. (7) as given following [40,43]:

$$N_{ss} = \frac{1}{q}\left[\frac{\varepsilon_i}{\delta}(n(V) - 1) - \frac{\varepsilon_s}{W_D}\right] \tag{7}$$

In formula 7; ε_s is the permittivity of the semiconductor, ε_i is the permittivity of the interface layer, W_D is the depletion layer width, and δ is the thickness of the interface layer. Card and Rhoderick are indicated that the energy of the interfacial states (E_{ss}) in p-type semiconductors and the valence band edge (E_V) are calculated by Eq. (8) [43,44]:

$$E_{ss} - E_v = q(\Phi_e - V) \tag{8}$$

Thus, the energy-dependent profiles of N_{ss} for SDs were calculated from Eqs. (7) and (8) by using the forward bias I–V data by taking into account voltage-dependent of ideality factor (n(V)) and effective BH (Φe) and as given in Eq. (9) and Eq. (10) [38,44,52]:

$$n(V) = \frac{q(V - IRs)}{kT.\ln\left(\frac{I_i}{I_{io}}\right)} \tag{9}$$

$$\Phi_e = \Phi_{BO} + \beta(V - IR_s) = \Phi_{BO} + \left(1 - \frac{1}{n(V)}\right)(V - IR_s) \tag{10}$$

Fig. 7 shows the N_{ss} vs (E_{ss}-E_v) for the fabrication of the SDs in dark cases. The value of n in MS is higher than the others which can be attributed to the existence of N_{ss}, ZnO:Si_3N_4 layer, voltage-dependent BH and a spatial barrier-inhomogeneity at MS interface due to the native SiO_2 layer [43,44]. Max and min N_{ss} values of the samples were given in Table 2.

The decrease of the gaps between grains contributed to the decrease in the surface-states/interface traps, some dislocations or impurities due to doping acceptor atoms, some disorders density of in the crystal structure, and some inorganic-dirties in the laboratory environment during the fabrication processes. They are usually located between the interfacial layer and p-Si within the energy band gap of the semiconductor and show almost U shape behaviour dependent on a special distribution of them between the interface layer and semiconductor in the forbidden band gap of Si [53]. They usually increase from the mid-gap of Si towards to bottom of the valence band almost as exponentially. The values of N_{ss} for the SDs are lower than due to the passivation effect of Si_3N_4 in the dark. With the addition of Si_3N_4, the surface states are reordered by reconstruction of microstructure [31,52] and it supports explaining the electrical performance of the MIS2 and why it is the best one of the samples.

4. Conclusions

The junction properties of Al/p-Si SDs with ZnO and ZnO:Si_3N_4 nanocomposite interface layers have been investigated by various I–V methods. Al/ZnO:Si_3N_4/p-Si SD has a metal-insulator layer-semiconductor configuration rather than an ideal SD. The basic diode parameters (n, Φb, R_s and R_{sh}) were determined from TE, Norde, and

Table 1
Comparison of the different obtained basic diode parameters of the samples in dark.

Sample	Ideality (n)		Φ_b (eV)			R_{sh} (kΩ)	R_s (kΩ)			
	TE	dV/dLnI	TE	Norde	dV/dLnI	Ohm's Law	Ohm's Law	Norde	dV/dLnI	H(I)
MS	4.58	6	0.66	0.66	0.64	20	4.65	2.73	3.64	3.04
MIS1	4.26	5.2	0.60	0.62	0.60	145	2.47	1.48	1.84	2.88
MIS2	3.85	4.8	0.55	0.58	0.56	258	0.65	0.16	0.23	0.78

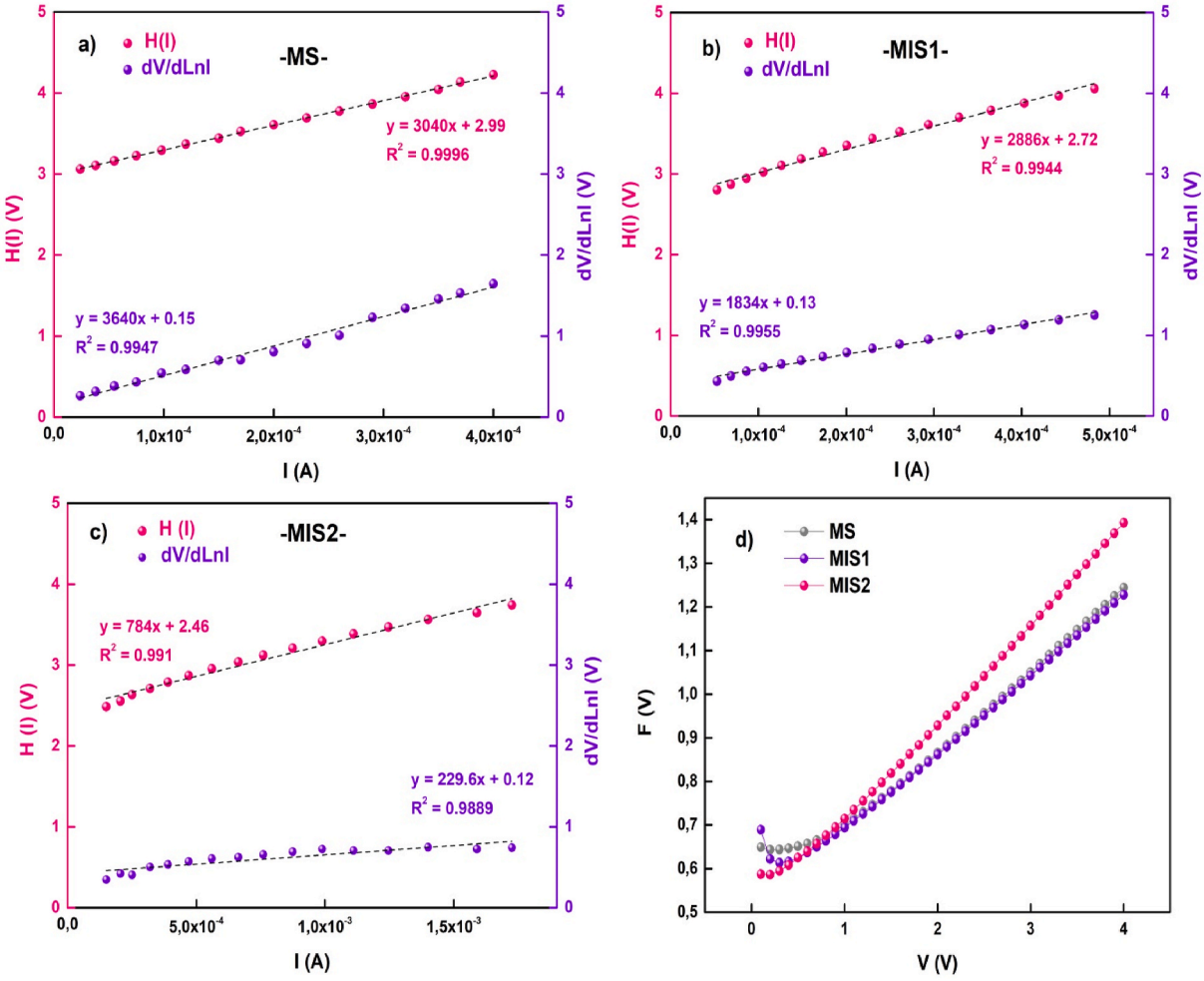

Fig. 6. The H(I)–I and dV/dLnI-I plots of a) MS, b) MIS1, c) MIS2 samples, and d) F(V)–V plots.

Table 2
Comparison of the Nss values of the samples in dark.

Sample	N_{ss} ($eV^{-1}.cm^{-2}$) Card-Roderick		E_{ss} - E_v (eV)	
	Min	Max	Min	Max
MS	1.56×10^{13}	6.42×10^{13}	0.46	0.59
MIS1	1.11×10^{12}	4.78×10^{12}	0.44	0.55
MIS2	1.08×10^{12}	2.15×10^{12}	0.43	0.52

Cheung functions and compared with each other. The n values were found 4.58, 4.26, 3.85 from TE and 6, 5.2, 4.8 from dV/dLnI vs I plots for the MS, the MIS1, and the MIS2 samples, respectively. The lowest R_s values were calculated as 0.65, 0.16, 0.23, and 0.78 kΩ by various methods for MIS2 and given in detail. The MIS2 sample has the highest R_{sh} values extracted from the reverse bias region of I–V curves and R_i-V plots by calculation with Ohm's Law as 258 kΩ.

The Φ_b values were obtained as 0.66, 0.60 and 0.55 eV for MS, MIS1 and MIS2 with the TE method, and also calculated by different methods. It was decreased with doping of the Si_3N_4 and provided to increase in conduction with the help of reconstruction of microstructure.

The energy distribution of the interface states has been extracted from the I–V data. The density of interface states has been calculated as (1.56–6.42)x10^{13}, (1.11–4.78)x10^{12} and (1.08–2.15)x10^{13} eV^{-1} cm^{-2} for the MS, the MIS1, and the MIS2 samples, respectively. Referring to all these properties of the MIS2 SD, it has the best basic diode parameters and it can be said that ZnO:Si_3N_4 nanocomposite can be promising as an insulating material for optoelectronic devices.

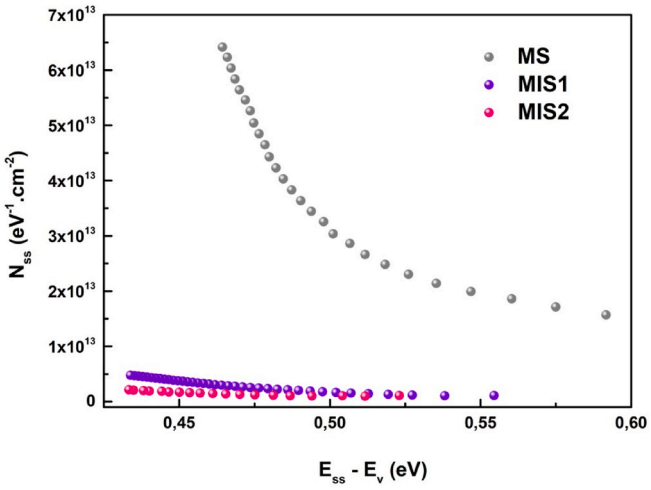

Fig. 7. The N_{ss} – (E_{ss}-E_v) curves of the MS, MIS1 and MIS2 structures.

Credit author statement

Erhan İbrahimoğlu: Experimental measurements, Investigation, Writing – review & editing.**Mine Kırkbınar**: Experimental

measurements, Investigation, Writing – review & editing. **Fatih Çalışkan**: Review & editing, Supervision. **Zafer Tatlı**: Review & editing, Supervision.

Declaration of competing interest

The authors declare that they have no known competing financial interests or personal relationships that could have appeared to influence the work reported in this paper.

Data availability

No data was used for the research described in the article.

Acknowledgements

The study was funded by Sakarya University of Applied Sciences Scientific Research Projects (Project Number: 070–2022).

References

[1] Y.K. Mishra, V.S.K. Chakravadhanula, V. Hrkac, S. Jebril, D.C. Agarwal, S. Mohapatra, D.K. Avasthi, L. Kienle, R. Adelung, Crystal growth behaviour in Au-ZnO nanocomposite under different annealing environments and photoswitchability, J. Appl. Phys. 112 (2012), 064308.
[2] P.A. Rodnyi, I.V. Khodyuk, Optical and luminescence properties of zinc oxide, Opt. Spectrosc. 111 (2011) 776.
[3] H. Wang, X. Mo, Z. Chen, S. Li, H. Huang, Y. Liu, G. Fang, Near white electro-luminescence from self-supporting ZnO nanocone array based heterojunction light-emitting diodes, Mater. Res. Express 2 (2015), 035005, https://doi.org/10.1088/2053-1591/2/3/035005.
[4] A. Janotti, C.G. Van de Walle, Fundamentals of zinc oxide as a semiconductor, Rep. Prog. Phys. 72 (2009), 126501.
[5] X. Wen, J.A. Davis, L.V. Dao, P. Hannaford, V.A. Coleman, H.H. Tan, C. Jagadish, K. Koike, S. Sasa, M. Inoue, M. Yano, Thermal quenching of photoluminescence in ZnO/ZnMgO multiple quantum wells following oxygen implantation and rapid thermal annealing, J. Lumin. 129 (2009) 153, https://doi.org/10.1016/j.jlumin.2008.09.006.
[6] H.D. Sun, T. Makino, Y. Segawa, Enhancement of exciton binding energies in ZnO/ZnMgO multi quantum wells, J. Appl. Phys. 91 (2002) 1993.
[7] W. Xu, Z. Ye, Y. Zeng, L. Zhu, B. Zhao, L. Jiang, J. Lu, H. He, S. Zhang, ZnO lightemitting diode grown by plasma-assisted metal organic chemical vapor deposition, Appl. Phys. Lett. 88 (17) (2006), 173506.
[8] R. Ahmad, N. Tripathy, M. Ahn, Y. Hahn, Highly stable hydrazine chemical sensor based on vertically-aligned ZnO nanorods grown on electrode, J. Colloid Interface Sci. 494 (2017) 153–158.
[9] O. Jamadi, F. Reveret, P. Disseix, F. Medard, J. Leymarie, A. Moreau, D. Solnyshkov, C. Deparis, M. Leroux, E. Cambril, et al., Edge-emitting polariton laser and amplifier based on a ZnO waveguide, Light Sci. Appl. 7 (1) (2018) 82.
[10] M. Patel, H. Kim, J. Kim, J. Yun, S. Kim, E. Choi, H. Park, Excitonic metal oxide heterojunction (NiO/ZnO) solar cells for all-transparent module integration, Sol. Energy Mater. Sol. Cells 170 (2017) 246–253.
[11] L. Agarwal, B. Singh, S. Tripathi, P. Chakrabarti, Fabrication and characterization of Pd/Cu doped ZnO/Si and Ni/Cu doped ZnO/Si Schottky diodes, Thin Solid Films 612 (2016) 259–266.
[12] S. Chu, M. Olmedo, Z. Yang, J. Kong, J. Liu, Electrically pumped ultraviolet ZnO diode lasers on Si, Appl. Phys. Lett. 93 (18) (2008), 181106.
[13] S. Liang, H. Sheng, Y. Liu, Z. Huo, Y. Lu, H. Shen, ZnO Schottky ultraviolet photodetectors, J. Cryst. Growth 225 (2–4) (2001) 110–113.
[14] M. Kırkbınar, E. İbrahimoğlu, A. Demir, Ş. Altındal, F. Çalışkan, Improvement of electric and photoelectric properties of the Al/n-ZnO/p-Si/Al photodiodes by green synthesis method using chamomille flower extract, J. Mater. Sci. Mater. Electron. 34 (3) (2023) 242, https://doi.org/10.1007/s10854-022-09515-9.
[15] M. Kırkbınar, A. Demir, Ş. Altındal, F. Çalışkan, The effect of different rates of ultra-thin gossamer-like rGO coatings on photocatalytic performance in ZnO core-shell structures for optoelectronic applications, Diam. Relat. Mater. 130 (2022), 109435, https://doi.org/10.1016/j.diamond.2022.109435.
[16] Y. Wei, L. Ke, J. Kong, H. Liu, Z. Jiao, X. Lu, et al., Enhanced photoelectrochemical water-splitting effect with a bent ZnO nanorod photoanode decorated with Ag nanoparticles, Nanotechnology 23 (2012), 235401.
[17] M.C. Huang, J.C. Lin, S.H. Cheng, W.H. Weng, Influence of Gadopant on photoelectrochemical characteristic of Ga-doped ZnO thin films deposited by solegel spin-coating technique, Surf. Interface Anal. 49 (2016) 434e40.
[18] C. Wang, Y. Feng, L. Cai, X. Yang, J. He, W. Yan, et al., ZnO@ Sdoped ZnO core/shell nanocomposites for highly efficient solar water splitting, J. Power Sources 269 (2014) 24e30.
[19] C.J. Lin, L.C. Kao, Y. Huang, M.A. Banares, S.H. Liou, Uniform deposition of coupled CdS and CdSe quantum dots on ZnO nanorod arrays as electrodes for photoelectrochemical solar water splitting, Int. J. Hydrogen Energy 40 (2015) 1388e93.
[20] S. Sharma, S. Singh, N. Khare, Enhanced photosensitization ofzinc oxide nanorods using polyaniline for efficientphotocatalytic and photoelectrochemical water splitting, Int. J. Hydrogen Energy 41 (2016) 21088e98.
[21] A. Rokade, S. Rondiya, V. Sharma, M. Prasad, H. Pathan, S. Jadkar, Electrochemical synthesis of 1D ZnOnanoarchitectures and their role in efficient photoelectrochemical splitting of water, J. Solid State Electrochem. (2016) 1e10.
[22] H. Chen, Z. Wei, K. Yan, Y. Bai, Z. Zhu, T. Zhang, et al., Epitaxial growth of ZnO Nanodisks with large exposed polar facets onnanowire arrays for promoting photoelectrochemical water splitting, Small 10 (2014) 4760e9.
[23] A. Zerr, G. Miehe, G. Serghiou, M. Schwarz, E. Kroke, R. Riedel, H. Fuess, P. Kroll, R. Boehler, Synthesis of. cubic silicon nitride, Lett. Nature 400 (1999) 340–342.
[24] O. Blázquez, J. López-Vidrier, S. Hernández, J. Montserrat, B. Garrido, Electro-optical Properties of Non-stoichiometric Silicon Nitride Films for Photovoltaic Applications, Energy Procedia, 2013.
[25] V.V. Ichenko, V.V. Marin, S.D. Lin, K.Y. Panarn, A.A. Buyanin, O.V. Tretyak, Room temperature negative differential capacitance in self-assembled quantum dots, J. Phys. D Appl. Phys. 41 (2008), 235107.
[26] G.B. Sakr, I.S. Yahia, Effect of illumination and frequency on the capacitance spectroscopy and the relaxation process of p-ZnTe/n-CdMnTe/GaAs magnetic diode for photocapacitance applications, J. Alloys Compd. 503 (2010) 213–219.
[27] B.H. Lee, L. Kang, R. Nieh, W.J. Qi, J.C. Lee, Thermal stability and electrical characteristics of ultrathin hafnium oxide gate dielectric reoxidized with rapid thermal annealing, Appl. Phys. Lett. 76 (2000) 1926.
[28] N. Park, C. Choi, T. Seong, S. Park, Quantum confinement in amorphous silicon quantum dots embedded in silicon nitride, Phys. Rev. Lett. 86 (2001) 1355.
[29] M. Vila, C. Prieto, P. Miranzo, M.I. Osendi, R. Ramirez, Characterization of SiN thin films prepared by r.f. magnetron sputtering, Surf. Coating. Technol. (2002) 67–71, 151 – 152.
[30] M.M. Bülbül, S. Zeyrek, S. Altındal, H. Yüzer, On the profile of temperature dependent series resistance in Al/Si_3N_4/p-Si (MIS) Schottky diodes, Microelectron. Eng. 83 (2006) 577–581.
[31] G. Sharma, A. Kumar, S. Sharma, Mu Naushad, P. Dhiman, Dai-V.N. Vo, F. J. Stadler, Fe_3O_4/ZnO/Si_3N_4 nanocomposite based photocatalyst for the degradation of dyes from aqueous solution, Mater. Lett. 278 (2020), 128359.
[32] F. Çalışkan, A. Demir, Z. Tatlı, Fabrication of Si_3N_4 Preforms From Si_3N_4 Produced via CRN Technique, Journal of Porous Materials 20 (2013) 1501–1507.
[33] Q. Yang, D. Zhang, Z. Li, W. Luo, L. Pan, Influence of surface step width of 4H-SiC substrates on the GaN crystal quality, J. Cryst. Growth 504 (2018) 41–43.
[34] M. Ghorbani, H. Abdizadeh, M. Taheri, M.R. Golobostanfard, Enhanced photoelectrochemical water splitting inhierarchical porous ZnO/Reduced graphene oxide nanocomposite synthesized by sol-gel method, Hydrogen Energy 43 (2018) 7754–7763.
[35] P.C. Wuytens, A.G. Skirtach, R. Baets, On-chip surface-enhanced Raman spectroscopy using nanosphere-lithography patterned antennas on silicon nitride waveguides, Opt Express 25 (2017) 12926–12934.
[36] W.C. Ding, D. Hu, J. Zheng, P. Chen, B.W. Cheng, J.Z. Yu, Q.M. Wang, Strong visible and infrared photoluminescence from Er-implanted silicon nitride films, Journal Of Physıcs D: Appl. Phys. 41 (2008), 135101.
[37] J. Zi, H. Buscher, C. Falter, W. Ludwig, K. Zhang, X.D. Xie, Raman shifts in Si nanocrystals, Appl. Phys. Lett. 69 (1996) 200.
[38] H. Agarwal, S. Venkat Kumar, S. Rajeshkumar, A review on green synthesis of zinc oxide nanoparticles – an eco-friendly approach, Resource-Efficient Technologies 3 (2017) 406–413.
[39] S.M. Sze, M.K. Lee, Semiconductor Devices: Physics and Technology, third ed., Wiley, Hoboken, N.J, 2013.
[40] H.C. Card, E.H. Rhoderick, Studies of tunnel MOS diodes I. Interface effects in silicon Schottky diodes, J. Phys. D Appl. Phys. 4 (10) (1971) 1589–1601.
[41] W. Chebil, A. Gokarna, A. Fouzri, N. Hamdaoui, K. Nomenyo, G. Lerondel, Study of the growth time effect on the structural, morphological and electrical characteristics of ZnO/p-Si heterojunction diodes grown by sol-gel assisted chemical bath deposition method, J. Alloys Compd. 771 (2019) 448–455.
[42] Sh A. Mansour, F. Yakuphanoglu, Electrical-optical properties of nanofiber ZnO film grown by sol gel method and fabrication of ZnO/p-Si heterojunction, Solid State Sci. 4 (2012) 121–126.
[43] J. Farazin, M.S. Asi, G. Pirgholi-Givi, S.A. Delbari, A.S. Namini, Ş. Altındal, Y. Azizi-Kalandaragh, Effect of (Co-TeO_2 – doped polyvinylpyrrolidone) organic interlayer on the electrophysical characteristic of Al/p-Si (MS) structures, J. Mater. Sci. Mater. Electron. 32 (2021) 21909–21922.
[44] Ş. Altındal, A. Barkhordari, G. Pirgholi-Givi, M. Ulusoy, H. Mashayekhi, S. Ozcelik, Y. Azizi-Kalandaragh, Comparison of the electrical and impedance properties of Au/(ZnOMn:PVP)/n-Si (MPS) type Schottky-diodes (SDs) before and after gamma-irradiation, Phys. Scripta 96 (2021), 125881.
[45] Y. Choi, K. Lee, C.H. Park, K. H Lee, J.W. Nam, M. M Sung, K.M. Lee, H.C. Sohn, S. Im, High current fast switching n-ZnO/p-Si diode, J. Phys. D Appl. Phys. 43 (2010), 345101.
[46] F. Yakuphanoglu, Y. Caglar, M. Caglar, S. Ilican, ZnO/p-Si heterojunction photodiode by sol–gel deposition of nanostructure n-ZnO film on p-Si substrate, Mater. Sci. Semicond. Process. 13 (2010) 137–140.
[47] S. Aksoy, Y. Caglar, Effect of ambient temperature on electrical properties of nanostructure n-ZnO/p-Si heterojunction diode, Superlattice. Microst. 51 613 (2012) 625.
[48] S. Mridha, M. Dutta, D. Basak, Photoresponse of n-ZnO/p-Si heterojunction towards ultraviolet/visible lights: thickness dependent behavior, Mater. Sci.: Mater Electron 20 (2009) 376–379.
[49] H. Sun, Q.F. Zhang, J.L. Wu, Electroluminescence from ZnO nanorods with an n-ZnO/p-Si heterojunction structure, Nanotechnology 17 (2006) 2271–2274.

[50] N. Zebbar, Y. Kheireddine, K. Mokeddem, A. Hafdallah, M. Kechouane, M.S. Aida, Structural, optical and electrical properties of n-ZnO/p-Si heterojunction prepared by ultrasonic spray, Mater. Sci. Semicond. Process. 14 (2011) 229–234.
[51] S. Sharma, C. Periasamy, A study on the electrical characteristic of n-ZnO/p-Si heterojunction diode prepared by vacuum coating technique, Superlattice. Microst. 73 (2014) 12–21.
[52] N. Soylu Koc, S.P. Altintas, M. Gokcen, M. Dogruer, C. Altug, A. Varilci, Current-voltage characteristics of nano whisker ZnO/Si heterojunction under UV exposition, Sensor Actuator Phys. 342 (2022), 113618.
[53] L. Chabane, N. Zebbar, M. Trari, Y.H. Seba, M. Kechouane, Electrical study of ZnO film thickness effect on the evolution of interface potential barrier of ZnO/p-Si heterojunction: contribution to transport phenomena study, Mater. Sci. Semicond. Process. 133 (2021), 105971.